Polarity reversal of wakefields driven by ultrashort pulse laser

P. Valenta,[1,2,*] T. Zh. Esirkepov,[3] J. K. Koga,[3] A. Nečas,[4] G. M. Grittani,[1] C. M. Lazzarini,[1] O. Klimo,[1,2] G. Korn,[1] and S. V. Bulanov[1,3]

[1]*ELI Beamlines, Institute of Physics of the Czech Academy of Sciences, Na Slovance 2, Prague 18221, Czech Republic*

[2]*Faculty of Nuclear Sciences and Physical Engineering, Czech Technical University in Prague, Brehova 7, Prague 11519, Czech Republic*

[3]*Kansai Photon Science Institute, National Institutes for Quantum and Radiological Science and Technology, Umemidai 8-1-7, Kizugawa, Kyoto 619-0215, Japan*

[4]*TAE Technologies, Pauling 19631, Foothill Ranch, California 92610, USA*

(Received 7 July 2020; revised 3 September 2020; accepted 25 October 2020; published 30 November 2020)

Using an analytical model and computer simulation, we show that the wakefield driven by an ultrashort laser pulse in high-density plasma periodically reverses its polarity due to the carrier-envelope phase shift of the driver. The wakefield polarity reversal occurs on spatial scales shorter than the typical length considered for electron acceleration with the laser-wakefield mechanism. Consequently, the energies of accelerated electrons are significantly affected. The results obtained are important for the laser-wakefield acceleration under the conditions relevant to present-day high-repetition-rate laser systems.

DOI: 10.1103/PhysRevE.102.053216

I. INTRODUCTION

Laser-wakefield acceleration (LWFA) is a well-established technique for producing high-energy electrons in plasma [1,2]. Over the past few decades, the quality of electron beams accelerated via LWFA has rapidly evolved mainly due to the advances in technology and better understanding of the underlying physics. As of 2020, LWFA has demonstrated (although not simultaneously) the capability to produce electron beams at the multi-GeV energy scale with a relative energy spread of a few percent [3,4], a few fs duration [5–8], and hundreds of pC of charge [9,10]. These achievements make LWFA increasingly attractive for a wide range of multidisciplinary experiments and applications (e.g., radiography [11], radiotherapy [12], and radiolysis [12,13]).

Recently, there has been a growing interest in LWFA driven by high-repetition-rate ($\gtrsim$kHz) laser systems since they can significantly improve certain characteristics (e.g., stability, signal-to-noise ratio, and average electron current [14]) required by a number of practical applications (e.g., ultrafast electron diffraction [15,16], fs x-ray generation [17,18], and pulsed radiolysis [19]). In order to produce high-quality relativistic LWFA electron sources with present-day kHz lasers, one should use tightly focused, near-single-cycle pulses and thin, near-critical density gas targets [14,20]. Such considerations constitute a great challenge not only from a technical point of view, but also in the sense of the understanding of underlying physical processes (e.g., related to the λ^3 regime [21]).

The LWFA of electrons at kHz using laser pulses with energies $<$10 mJ has been pursued by several groups [22–24]. The specificities of the corresponding laser-plasma interaction, particularly the effects of the driver carrier-envelope phase (CEP) on the electron beam dynamics [25], the electron injection [26], and the electron energy spectra [14,27], were investigated. In this paper, we present the results of analytical and numerical study of the wakefield driven by an ultrashort laser pulse in high-density plasma. We show that the wakefield polarity periodically reverses due to the CEP shift of the driving pulse which significantly affects the energies of electrons accelerated via LWFA under the conditions relevant to current high-repetition-rate lasers.

II. DISPERSION AND CARRIER-ENVELOPE PHASE SHIFT EFFECTS

The propagation of a small amplitude electromagnetic wave in collisionless plasma is governed by the dispersion equation $\omega^2 = 1 + k^2$. The frequency, ω, and wave number, k, of the electromagnetic wave are measured in the units of ω_p and ω_p/c, respectively, where $\omega_p = \sqrt{4\pi n_0 e^2/m_e}$ is the Langmuir frequency, c is the speed of light in vacuum, n_0 is the ambient electron number density, e is the elementary charge, and m_e is the electron mass. The phase and group velocities of the electromagnetic wave (in the units of c) are equal to $\beta_{\rm ph} = \sqrt{1+k^2}/k$ and $\beta_g = k/\sqrt{1+k^2}$, respectively. As one may see, $\beta_{\rm ph}\beta_g = 1$.

In dispersive media, the phase and group velocities are not equal to each other, $\beta_{\rm ph} \neq \beta_g$, which causes the evolution of the driver CEP. The characteristic time scale of the CEP shift effects can be expressed by a typical dispersion time, $t_{\rm disp}$, defined as the time span needed to acquire the CEP shift of the driver equal to π,

$$t_{\rm disp} = \pi/\omega(\beta_{\rm ph} - \beta_g) = \pi\beta_g/\omega\left(1-\beta_g^2\right). \tag{1}$$

The driver field during the time interval $<t_{\rm disp}$ can be in one-dimensional (1D) geometry approximated by the vector

*petr.valenta@eli-beams.eu

potential of the following form:

$$a = a_0 \frac{\sin\left[\Delta k(x-\beta_g t)\right]}{\Delta k(x-\beta_g t)} \cos\left[k_c(x-\beta_{\rm ph} t)+\varphi\right]. \quad (2)$$

Here, a_0 is the peak vacuum amplitude of the driver normalized by $m_e c^2/e$ and φ is the phase of the carrier wave. The driver wave numbers are assumed to lie within a finite band $k_c - \Delta k < k < k_c + \Delta k$, with $\Delta k \ll k_c$. The spatial coordinate, x, and time, t, are measured in units of c/ω_p and ω_p^{-1}, respectively.

While propagating in plasma, the driver excites a wakefield that can be described by the following system of equations [2]:

$$\partial_t p + v\partial_x p = -E + F, \quad (3)$$

$$\partial_t E + v\partial_x E = v. \quad (4)$$

Here p is the x component of the electron momentum normalized by $m_e c$, E is the x component of the electric field normalized by $E_p = m_e\omega_p c/e$, and $v = p/\gamma$ with γ being the electron Lorentz factor. This yields

$$F = -(1/2\gamma)\partial_x a^2 \quad (5)$$

for the driving force (in the units of $m_e\omega_p c$) with $a(x,t)$ given by Eq. (2). The transverse component of the generalized momentum is conserved (i.e., $p_\perp - a = \text{const}$) and, therefore, $\gamma = \sqrt{1+a^2+p^2}$. In the following, we assume that $\gamma = 1$ (i.e., the laser-plasma interaction regime is well below the wake wave breaking threshold). The nonlinear case is addressed by numerical simulation in the second part of the paper.

The system of Eqs. (3) and (4) can be solved, e.g., using Lagrange coordinates, x_0 and τ. The relation between the Euler and Langrange coordinates is defined as $t = \tau$ and $x = x_0 + \xi(x_0,\tau)$, where x_0 is the initial coordinate of the fluid element (at $t = 0$) and ξ is a displacement of the fluid element from its initial position, x_0, to the point x during the time t; thus $\partial_\tau \xi = v$. Assuming that $\xi \ll x_0$, the solution in quadratures reads

$$p + iE = \int_0^\tau \frac{a_0^2 k_c}{2} e^{i(\tau-\tau')} \left(\frac{\sin\left[\Delta k(x_0-\beta_g\tau')\right]}{\Delta k(x_0-\beta_g\tau')}\right)^2 \times \sin\left[2k_c\left(x_0-\beta_g^{-1}\tau'\right)+2\varphi\right] d\tau'. \quad (6)$$

In the ultrashort driver pulse limit, the solution (being transformed back to the Euler coordinates) becomes

$$p = -\frac{a_0^2}{2\beta_g}\frac{k_c}{\Delta k}\cos\left(\frac{x-\beta_g t}{\beta_g}\right)\sin\left(2k_c\frac{1-\beta_g^2}{\beta_g^2}x - 2\varphi\right), \quad (7)$$

$$E = \frac{a_0^2}{2\beta_g}\frac{k_c}{\Delta k}\sin\left(\frac{x-\beta_g t}{\beta_g}\right)\sin\left(2k_c\frac{1-\beta_g^2}{\beta_g^2}x - 2\varphi\right), \quad (8)$$

where $0 < x \leqslant \beta_g t$ and $t \geqslant 0$.

As can be seen from Eqs. (7) and (8), the ultrashort driver pulse in plasma excites the wakefield of a wavelength $\lambda_w = 2\pi\beta_g$ propagating with the phase velocity, β_w, equal to the group velocity of the driver, $\beta_w = \beta_g$. In addition to the standard model, the wakefield contains a sinusoidal modulation of the amplitude due to the slippage of the driver CEP. The modulation wavelength, given by $\lambda_{\rm mod} = \pi\beta_g^2/k_c(1-\beta_g^2)$, corresponds to the propagation length of the driver required to shift its CEP by the factor of π [compare with Eq. (1)]. As a consequence, the wakefield polarity periodically reverses. The range between two adjacent longitudinal coordinates at which the wakefield polarity reversal occurs is expressed by the polarity reversal length,

$$L_{\rm pr} = \lambda_{\rm mod}/2 = \pi\beta_g^2/2k_c\left(1-\beta_g^2\right). \quad (9)$$

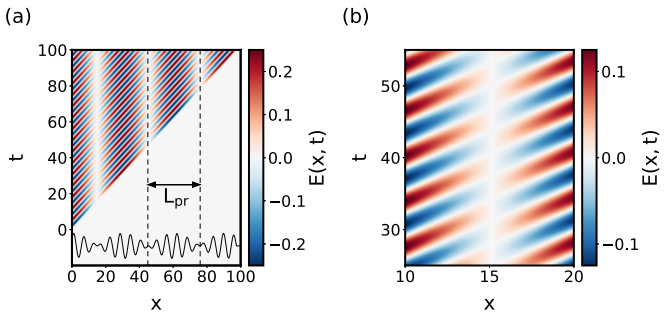

FIG. 1. Wakefield, $E(x,t)$, distribution in the (x,t) plane according to Eq. (8). The parameters of the driver are $\beta_g = 0.975$, $a_0 = 0.5$, $k_c = 1$, $\Delta k = 0.5$, and $\varphi = 3\pi/4$ and the plasma is homogeneous with $n_0 = 0.5 n_c$. Panel (a) shows the periodic reversal of the wakefield polarity with $L_{\rm pr} \simeq 30.24$ (marked by dashed lines); the detail of the wakefield polarity reversal is shown in (b). The solid line at the bottom of (a) shows the line-out of the wakefield along the axis $t = 100$.

Figure 1 shows the wakefield distribution in the (x,t) plane according to Eq. (8). The parameters of the driver are $\beta_g = 0.975$, $a_0 = 0.5$, $k_c = 1$, $\Delta k = 0.5$, and $\varphi = 3\pi/4$ and the plasma is homogeneous with $n_0 = 0.5 n_c$, where $n_c = n_0\omega^2$ stands for the critical plasma density. In panel (a), one may see the periodic reversal of the wakefield polarity with $L_{\rm pr} \simeq 30.24$. Panel (b) shows the detail of the wakefield polarity reversal.

III. ELECTRON ACCELERATION BY MODULATED WAKEFIELD

As is well known, the energy of the LWFA accelerated electron is limited by the value determined by the dephasing length,

$$L_d = \pi\beta_g/(1-\beta_g). \quad (10)$$

Following from the model, the polarity reversal length is (in underdense plasma) always shorter than the dephasing length, $L_{\rm pr} < L_d$. A comparison between $L_{\rm pr}$ and L_d defined by Eqs. (9) and (10), respectively, is shown in Fig. 2.

The wakefield polarity reversal in its turn affects the energy of the accelerated electron. For illustration, let us consider a relativistic electron traversing the wakefield with velocity approaching the speed of light. The net change of the kinetic energy of the electron moving along the path from $x_0 = 0$ to

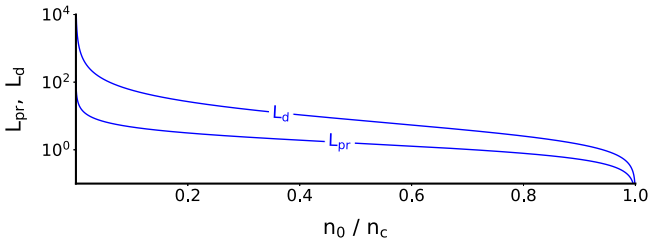

FIG. 2. Comparison between the polarity reversal length, $L_{\rm pr}$, and the dephasing length, L_d, defined by Eqs. (9) and (10), respectively, in the whole range of underdense plasma.

$x_1 = x$ (in the units of $m_e c^2$) is given by

$$\Delta\mathcal{E}(x) = \int_0^x E(x', t = x')dx' = \frac{a_0^2}{4\beta_g}\frac{k_c}{\Delta k}\frac{\cos(\alpha^- x + 2\varphi)\sin(\alpha^- x)}{\alpha^-} - \frac{a_0^2}{4\beta_g}\frac{k_c}{\Delta k}\frac{\cos(\alpha^+ x - 2\varphi)\sin(\alpha^+ x)}{\alpha^+}, \quad (11)$$

with the coefficients α^+ and α^- equal to

$$\alpha^{\pm} = \frac{\pi}{2}\left(\frac{1}{L_d} \pm \frac{1}{L_{\rm pr}}\right). \quad (12)$$

The energy change of the electron described by Eq. (11) is shown in Fig. 3. The electron is traversing the wakefield given by Eq. (8) for the same parameters of the driver and plasma as in Fig. 1 (solid line). As can be seen, the electron either gains or loses energy over the distance of $L_{\rm pr} \simeq 30.24$ due to the periodic reversal of the wakefield polarity. The energy balance of the electron over $L_d \simeq 122.52$ is $\Delta\mathcal{E} \simeq -1.29$. Using the standard model (i.e., neglecting the wakefield polarity reversal), the electron would theoretically gain the energy of $\Delta\mathcal{E} \simeq 20$ over the same distance. Since $L_{\rm pr} \ll L_d$, the electron energy gain under the considered conditions is always lower than the maximum value determined by the standard model.

It follows from Eq. (11) that the energy gain depends on the initial phase of the driver, φ. Therefore, one may find (by examining the function extrema) an optimal phase of the driver, $\varphi_{\rm opt}$, for which the net energy acquired by the electron over given distance is maximal. Provided that the electron injection is localized at $x = 0$ and the acceleration takes place over L_d,

$$\varphi^n_{\rm opt} = \frac{\pi}{4}\left(1 + \frac{L_d}{L_{\rm pr}}\right) + n\pi, \quad n \in \mathbb{Z}. \quad (13)$$

The energy change of the electron for $\varphi = \varphi_{\rm opt}$ is shown in Fig. 3 by the dashed line.

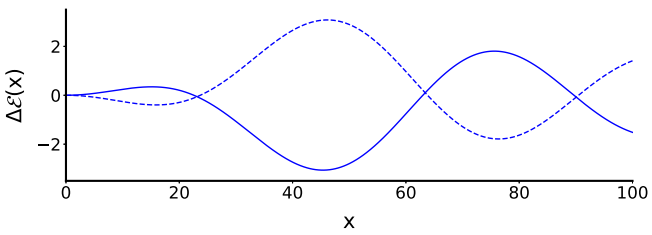

FIG. 3. Energy change of the relativistic electron, $\Delta\mathcal{E}(x)$, according to Eq. (11). The solid line shows the energy change of electron traversing the wakefield described by Eq. (8) for the same parameters of the driver and plasma as in Fig. 1. The dashed line shows the energy change of electron for $\varphi = \varphi_{\rm opt}$.

IV. PARTICLE-IN-CELL SIMULATION

A. Simulation setup

Now we explore the self-consistent evolution of the ultrashort laser pulse and near-critical density plasma numerically by means of particle-in-cell (PIC) simulation in a three-dimensional (3D) Cartesian geometry. The simulation is carried out using the PIC code EPOCH [28]. The driver laser pulse is characterized with the frequency $\omega_0 = 2\pi c/\lambda_0$, where λ_0 is its vacuum wavelength. The driver is Gaussian in both spatial and temporal profiles. Its peak normalized amplitude is $a_0 = 1.4$. It contains a single optical cycle, i.e., its full width at half maximum duration is $\tau_0 = 1\ T_0$, where $T_0 = \lambda_0/c$ is the cycle period of the driver. The beam waist, $w_0 = 4\lambda_0$, is chosen such that the Rayleigh length of the driver is sufficiently long, and thus enables one to capture the periodic nature of the wakefield polarity reversal.

The driver, being linearly polarized along the z axis, propagates along the x axis in a preionized homogeneous slab of a hydrogen plasma with electron and proton densities $n_{e,p} = 0.1 n_c$. The number of quasiparticles per cell is 4 for both particle species. The impact of the wakefield polarity reversal on the electron acceleration is studied using a beam of test electrons introduced through the left simulation boundary. The test electrons are initially monoenergetic with the Lorentz factor $\gamma_e = \sqrt{10}$, so that their velocity is comparable to the wake wave phase velocity (to fulfill the injection conditions).

The size of the simulation domain is $120\lambda_0$ in the laser propagation direction and $40\lambda_0$ in the transverse directions. The Cartesian grid is uniform with the resolution of 40 and 20 cells per λ_0 along the laser propagation direction and the transverse directions, respectively. The group velocity of the driving pulse in plasma can be roughly estimated as $v_g \simeq c\sqrt{1 - \omega_p^2/\omega_0^2} \simeq 0.95c$ and the wave number equals $k_c = \sqrt{\omega_0^2 - \omega_p^2}/c \simeq 5.96\lambda_0^{-1}$. This yields $L_{\rm pr} \simeq 2.37\lambda_0$ and $L_d \simeq 29.24\lambda_0$ for the polarity reversal and dephasing lengths defined by Eqs. (9) and (10), respectively.

B. Simulation results

Figure 4 shows the temporal evolution of the wakefield on the laser propagation axis, where one may clearly see that the wakefield polarity periodically reverses [panel (a)] as well as the detail of the wakefield polarity reversal [panel (b)]. The results of the PIC simulation qualitatively correspond to the analytical model derived above (compare with Fig. 1). Figure 5 shows the spatial distribution of the wakefield at time $t = 100T_0$, where one may see that the polarity reversal of the wakefield occurs only in the vicinity of the laser propagation axis.

The polarity reversal length, determined by measuring the range between two longitudinal coordinates at which

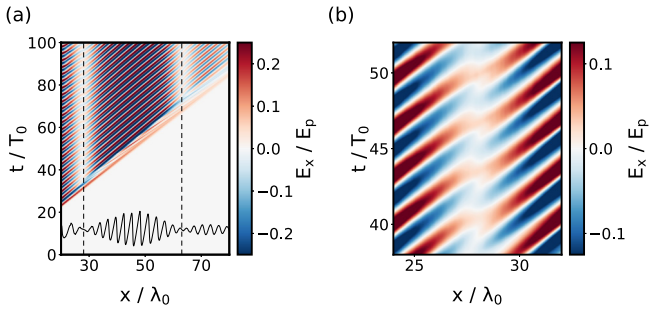

FIG. 4. Temporal evolution of the wakefield, E_x, on the laser propagation axis obtained from the 3D PIC simulation. Panel (a) shows the periodic reversal of the wakefield polarity with $L_{\rm pr} \simeq 35\lambda_0$ (marked by dashed lines); the detail of the wakefield polarity reversal is shown in (b). The solid line at the bottom of (a) shows the line-out of the wakefield along the axis $t = 100T_0$.

the wakefield polarity reverses, is $L_{\rm pr} \simeq 35\lambda_0$. We note that the value of $L_{\rm pr}$ as observed in the simulation differs from the analytical prediction. This could be due to several reasons: (i) the analytical model is 1D; (ii) the driver pulse amplitude is larger than unity and thus the interaction is not in the linear regime; (iii) although the driver pulse initially consists of a single optical cycle, it is not infinitely short. Moreover, it rapidly evolves into multiple cycles during the propagation in plasma due to the dispersion.

In Fig. 6, one can see the phase space of the test electrons, the on-axis wakefield, and the on-axis driver electric field at four successive instants of time. After traversing the plane of the wakefield polarity reversal, the electrons initially located in the accelerating phase of the wakefield start to decelerate (and vice versa). This leads to significant changes in the electron energies. As can be seen from the corresponding energy spectra, the energy of electrons initially located on the top of the phase space separatrix increases by $\simeq$15%.

The presented simulation indicates that, in the nonlinear regime, there may exist a case for which $L_{\rm pr} \simeq L_d$. In such a case, the dephasing limit is overcome and the electrons are accelerated until the energy of the driver pulse fully depletes.

V. CONCLUSION

In conclusion, we reveal the properties of the wakefield driven by an ultrashort laser pulse in high-density plasma. The analytical model and PIC simulation show that the wakefield under the considered conditions periodically reverses its polarity. This phenomenon is caused by the effects of dispersion and the CEP shift of the driver which are otherwise negligible in the case of a long pulse and relatively low-density plasma. The wakefield polarity reversal occurs on spatial scales shorter than the dephasing length and, therefore, significantly affects the energies of accelerated electrons. The study presented in this work is important for the LWFA under the conditions relevant to present-day high-repetition-rate lasers, where the results obtained are useful for better controlling of the parameters of accelerated electron beams (e.g., by adjusting the initial phase of the driver or by controlling the phase of the electron injection). We note that the described wake wave structure in high-density plasma could be observed in experiments by a new generation of laboratory diagnostics [29–31].

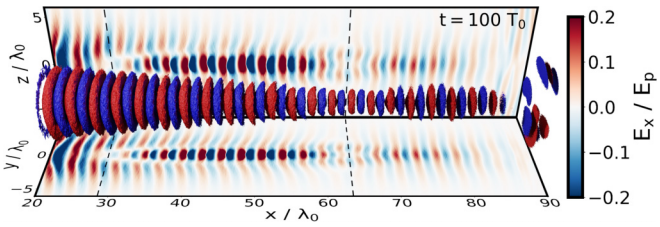

FIG. 5. Spatial distribution of the wakefield, E_x, at time $t = 100T_0$ obtained from the 3D PIC simulation. The dashed lines indicate the periodic reversal of the wakefield polarity with $L_{\rm pr} \simeq 35\lambda_0$.

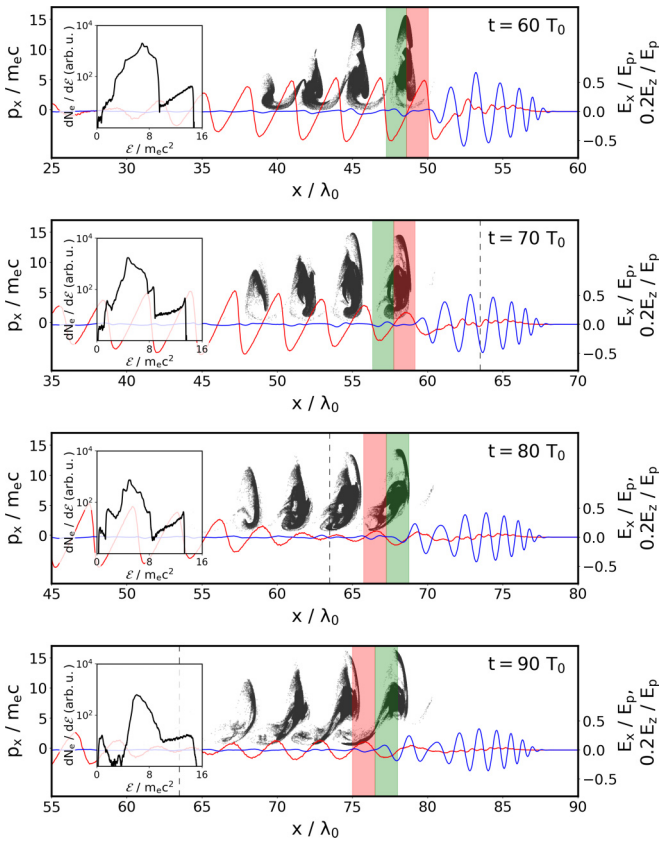

FIG. 6. (x, p_x) phase space of the test electrons (black), the on-axis wakefield, E_x (red), and the on-axis driver electric field, E_z (blue), at four successive time instants of the 3D PIC simulation. The corresponding inset shows the energy spectrum of electrons located in the first wake wave bucket behind the driver pulse, where N_e stands for the number of test electron quasiparticles. For the first wake wave bucket, the accelerating and decelerating phases of the wakefield are highlighted by green and red stripes, respectively. The longitudinal coordinate at which the wakefield polarity reversal occurs is marked by the dashed line.

ACKNOWLEDGMENTS

We appreciate discussions with Prof. H. Milchberg. This work was supported by the projects "High Field Initiative" (Grant No. CZ.02.1.01/0.0/0.0/15_003/0000449)

from the European Regional Development Fund and "IT4Innovations National Supercomputing Center" (Grant No. LM2015070) from the Ministry of Education, Youth and Sports of the Czech Republic. The EPOCH code was in part funded by the UK Engineering and Physical Sciences Research Council (EPSRC) Grants No. EP/G054950/1, No. EP/G056803/1, No. EP/G055165/1, and No. EP/M022463/1.

[1] T. Tajima and J. M. Dawson, Phys. Rev. Lett. **43**, 267 (1979).
[2] E. Esarey, C. B. Schroeder, and W. P. Leemans, Rev. Mod. Phys. **81**, 1229 (2009).
[3] H. T. Kim, K. H. Pae, H. J. Cha, I. J. Kim, T. J. Yu, J. H. Sung, S. K. Lee, T. M. Jeong, and J. Lee, Phys. Rev. Lett. **111**, 165002 (2013).
[4] A. J. Gonsalves, K. Nakamura, J. Daniels, C. Benedetti, C. Pieronek, T. C. H. de Raadt, S. Steinke, J. H. Bin, S. S. Bulanov, J. van Tilborg, C. G. R. Geddes, C. B. Schroeder, C. Tóth, E. Esarey, K. Swanson, L. Fan-Chiang, G. Bagdasarov, N. Bobrova, V. Gasilov, G. Korn, P. Sasorov, and W. P. Leemans, Phys. Rev. Lett. **122**, 084801 (2019).
[5] J. van Tilborg, C. B. Schroeder, C. V. Filip, C. Tóth, C. G. R. Geddes, G. Fubiani, R. Huber, R. A. Kaindl, E. Esarey, and W. P. Leemans, Phys. Rev. Lett. **96**, 014801 (2006).
[6] T. Ohkubo, A. Maekawa, R. Tsujii, T. Hosokai, K. Kinoshita, K. Kobayashi, M. Uesaka, A. Zhidkov, K. Nemoto, Y. Kondo, and Y. Shibata, Phys. Rev. ST Accel. Beams **10**, 031301 (2007).
[7] A. D. Debus, M. Bussmann, U. Schramm, R. Sauerbrey, C. D. Murphy, Z. Major, R. Hörlein, L. Veisz, K. Schmid, J. Schreiber, K. Witte, S. P. Jamison, J. G. Gallacher, D. A. Jaroszynski, M. C. Kaluza, B. Hidding, S. Kiselev, R. Heathcote, P. S. Foster, D. Neely, E. J. Divall, C. J. Hooker, J. M. Smith, K. Ertel, A. J. Langley, P. Norreys, J. L. Collier, and S. Karsch, Phys. Rev. Lett. **104**, 084802 (2010).
[8] O. Lundh, J. Lim, C. Rechatin, L. Ammoura, A. Ben-Ismaïl, X. Davoine, G. Gallot, J. P. Goddet, E. Lefebvre, V. Malka, and J. Faure, Nat. Phys. **7**, 219 (2011).
[9] Y. F. Li, D. Z. Li, K. Huang, M. Z. Tao, M. H. Li, J. R. Zhao, Y. Ma, X. Guo, J. G. Wang, M. Chen, N. Hafz, J. Zhang, and L. M. Chen, Phys. Plasmas **24**, 023108 (2017).
[10] J. P. Couperus, R. Pausch, A. Köhler, O. Zarini, J. M. Krämer, M. Garten, A. Huebl, R. Gebhardt, U. Helbig, S. Bock, K. Zeil, A. Debus, M. Bussmann, U. Schramm, and A. Irman, Nat. Commun. **8**, 487 (2017).
[11] Y. Glinec, J. Faure, L. Le Dain, S. Darbon, T. Hosokai, J. J. Santos, E. Lefebvre, J. P. Rousseau, F. Burgy, B. Mercier, and V. Malka, Phys. Rev. Lett. **94**, 025003 (2005).
[12] V. Malka, J. Faure, and Y. A. Gauduel, Mutat. Res. - Reviews Mutat. Res. **704**, 142 (2010).
[13] Y. A. Gauduel, Y. Glinec, J. P. Rousseau, F. Burgy, and V. Malka, Eur. Phys. J. D **60**, 121 (2010).
[14] J. Faure, D. Gustas, D. Guénot, A. Vernier, F. Böhle, M. Ouillé, S. Haessler, R. Lopez-Martens, and A. Lifschitz, Plasma Phys. Controlled Fusion **61**, 014012 (2019).
[15] G. Sciaini and R. J. Miller, Rep. Prog. Phys. **74**, 096101 (2011).
[16] R. J. Miller, Science **343**, 1108 (2014).
[17] K. Ta Phuoc, S. Corde, C. Thaury, V. Malka, A. Tafzi, J. P. Goddet, R. C. Shah, S. Sebban, and A. Rousse, Nat. Photon. **6**, 308 (2012).
[18] S. Corde, K. Ta Phuoc, G. Lambert, R. Fitour, V. Malka, A. Rousse, A. Beck, and E. Lefebvre, Rev. Mod. Phys. **85**, 1 (2013).
[19] Y. Muroya, M. Lin, Z. Han, Y. Kumagai, A. Sakumi, T. Ueda, and Y. Katsumura, Radiat. Phys. Chem. **77**, 1176 (2008).
[20] F. Salehi, A. J. Goers, L. Feder, B. Miao, D. Woodbury, and H. M. Milchberg, Rev. Sci. Instrum. **90**, 103001 (2019).
[21] G. Mourou, Z. Chang, A. Maksimchuk, J. Nees, S. V. Bulanov, V. Y. Bychenkov, T. Z. Esirkepov, N. M. Naumova, F. Pegoraro, and H. Ruhl, Plasma Phys. Rep. **28**, 12 (2002).
[22] Z. H. He, B. Hou, J. A. Nees, J. H. Easter, J. Faure, K. Krushelnick, and A. G. Thomas, New J. Phys. **15**, 053016 (2013).
[23] F. Salehi, A. J. Goers, G. A. Hine, L. Feder, D. Kuk, B. Miao, D. Woodbury, K. Y. Kim, and H. M. Milchberg, Opt. Lett. **42**, 215 (2017).
[24] D. Guénot, D. Gustas, A. Vernier, B. Beaurepaire, F. Böhle, M. Bocoum, M. Lozano, A. Jullien, R. Lopez-Martens, A. Lifschitz, and J. Faure, Nat. Photon. **11**, 293 (2017).
[25] E. N. Nerush and I. Y. Kostyukov, Phys. Rev. Lett. **103**, 035001 (2009).
[26] A. F. Lifschitz and V. Malka, New J. Phys. **14**, 053045 (2012).
[27] M. Ouillé, A. Vernier, F. Böhle, M. Bocoum, A. Jullien, M. Lozano, J. P. Rousseau, Z. Cheng, D. Gustas, A. Blumenstein, P. Simon, S. Haessler, J. Faure, T. Nagy, and R. Lopez-Martens, Light: Sci. Appl. **9**, 47 (2020).
[28] T. D. Arber, K. Bennett, C. S. Brady, A. Lawrence-Douglas, M. G. Ramsay, N. J. Sircombe, P. Gillies, R. G. Evans, H. Schmitz, A. R. Bell, and C. P. Ridgers, Plasma Phys. Controlled Fusion **57**, 113001 (2015).
[29] N. H. Matlis, S. Reed, S. S. Bulanov, V. Chvykov, G. Kalintchenko, T. Matsuoka, P. Rousseau, V. Yanovsky, A. Maksimchuk, S. Kalmykov, G. Shvets, and M. C. Downer, Nat. Phys. **2**, 749 (2006).
[30] M. C. Downer, R. Zgadzaj, A. Debus, U. Schramm, and M. C. Kaluza, Rev. Mod. Phys. **90**, 035002 (2018).
[31] T. Z. Esirkepov, J. Mu, Y. Gu, T. M. Jeong, P. Valenta, O. Klimo, J. K. Koga, M. Kando, D. Neely, G. Korn, S. V. Bulanov, and A. S. Pirozhkov, Phys. Plasmas **27**, 052103 (2020).